WPPFC-CPR(17) 17077

A Kirschner et al.

Modelling of plasma-wall interaction and impurity transport in fusion devices and prompt deposition of tungsten as application

Preprint of Paper to be submitted for publication in Proceeding of 44th European Physical Society Conference on Plasma Physics (EPS)

This work has been carried out within the framework of the EUROfusion Consortium and has received funding from the Euratom research and training programme 2014-2018 under grant agreement No 633053. The views and opinions expressed herein do not necessarily reflect those of the European Commission.

Modelling of plasma-wall interaction and impurity transport in fusion devices and prompt deposition of tungsten as application

A. Kirschner[1], D. Tskhakaya[2,3], S. Brezinsek[1], D. Borodin[1], J. Romazanov[1], R. Ding[4], A. Eksaeva[1,5], Ch. Linsmeier[1]

[1]*Forschungszentrum Jülich GmbH, Institut für Energie- und Klimaforschung – Plasmaphysik, 52425 Jülich, Germany*

[2]*Institute of Applied Physics, TU-Wien, A-1040 Vienna, Austria*

[3]*Andronikashvili Institute of Physics, 0177 Tbilisi, Georgia*

[4]*Institute of Plasma Physics, Chinese Academy of Sciences, P.O. Box 1126, Hefei, Anhui 230031, P.R. China*

[5]*National Research Nuclear University MEPhI, 31, Kashirskoe sh., 115409, Moscow, Russia*

Abstract

Main processes of plasma-wall interaction and impurity transport in fusion devices and their impact on the availability of the devices are presented and modelling tools, in particular the three-dimensional Monte-Carlo code ERO, are introduced. The capability of ERO is demonstrated on the example of tungsten erosion and deposition modelling. The dependence of tungsten deposition on plasma temperature and density is studied by simulations with a simplified geometry assuming (almost) constant plasma parameters. The amount of deposition increases with increasing electron temperature and density. Up to 100% of eroded tungsten can be promptly deposited near to the location of erosion at very high densities (~1e14 cm^{-3} expected e.g. in the divertor of ITER). The effect of the sheath characteristics on tungsten prompt deposition is investigated by using Particle-In-Cell simulations to spatially resolve the plasma parameters inside the sheath. Applying PIC data instead of non-resolved sheath leads in general to smaller tungsten deposition, which is mainly due to a density and temperature decrease towards the surface within the sheath. Two-dimensional tungsten erosion/deposition simulations, assuming symmetry in toroidal direction but poloidally spatially varying plasma parameter profiles, have been carried out for the JET divertor. The simulations reveal, similar to experimental findings, that tungsten gross erosion is dominated in H-mode plasmas by the intra-ELM phases. However, due to deposition, the net tungsten erosion can be similar within intra- and inter-ELM phases if the inter-ELM electron temperature is high enough. Also, the simulated deposition fraction of about 84% in between ELMs is in line with spectroscopic observations from which a lower limit of 50% has been estimated.

Keywords: plasma-wall interaction, erosion, prompt deposition, tungsten, ERO, JET

Corresponding author: A. Kirschner (a.kirschner@fz-juelich.de)

1. Introduction

The imperfect plasma confinement of magnetic fusion devices leads to the unavoidable interaction of ions and neutrals with the surrounding wall components. This so-called plasma-wall interaction (PWI) includes processes like physical sputtering, chemical erosion and deposition of eroded particles – an overview of the various erosion and deposition processes and the underlying physical and chemical mechanisms can be found in [1] and further references therein. The key PWI issues for ITER – the next step fusion device – are summarised in [2]. Corresponding experimental lessons learned so far from the JET tokamak, a proxy for ITER and equipped with the same material mixture, are described in [3]. The JET-ILW studies include fuel retention studies, which are of particular interest as a fusion machine will be operated with a 50-50 mixture of tritium and deuterium. Tritium retention by means of implantation or co-deposition within layers formed by deposition of eroded material is part of the PWI. The amount of the radioactive tritium retained within the wall components has to be kept below a certain value (e.g. 1 kg for ITER [4]) due to safety and fuel cycle reasons. These PWI processes thus may limit the wall components´ lifetime after which they have to be exchanged because of too large erosion or they have to be cleaned by elaborate measures to remove the retained tritium. The execution of both of these procedures is expensive and time consuming and thus has to be minimised for an economical operation of a reactor. Therefore, for future devices, predictions, minimisation, and control of the net erosion of wall components and the long-term tritium retention is important. For this purpose experimental studies at present machines in combination with modelling are indispensable.

The contribution at hand gives in section 2 an introduction of the three-dimensional Monte-Carlo code ERO, which is a well-established tool in fusion research to model PWI and impurity transport. Further modelling tools relevant to PWI studies will be briefly touched on.

As an application of the ERO code, prompt deposition of sputtered tungsten is studied in section 3.1. The influence of plasma density and temperature is explored. Moreover, the effect of the cut-off energy for the sputtered tungsten atoms is analysed. In many cases the characteristics of the sheath in front of the plasma-exposed surfaces is not considered in detail due to its small thickness. For instance, the plasma parameters (temperature, density, parallel flow velocity) are typically calculated up to the sheath entrance, whose position is set to the surface. To investigate the importance of the spatially resolved sheath characteristics, the output of Particle-In-Cell (PIC) simulations is used as an input for the ERO simulations. Resulting deposition is then compared with ERO modelling that neglects the detailed sheath characteristics. Finally, the calculated amounts of deposition for tungsten are compared to beryllium.

Section 3.2 is dedicated to tungsten erosion and deposition in the full W divertor of JET-ILW. The contribution of erosion from inter- and intra-ELM phases is estimated and compared with experimental observations made by optical emission spectroscopy. In addition, calculated prompt deposition is benchmarked with findings resulting from light emission of neutral and singly charged tungsten particles for the inter-ELM phase.

2. Modelling of plasma-wall interaction and impurity transport

2.1. Overview of common tools

A large number of various codes is available for modelling of the different aspects of plasma-wall interaction and impurity transport in fusion research. Here only a small selection is given

without any claim on completeness. Detailed description of these codes is out of the scope of this contribution and the reader is referred to the provided references.
So-called plasma simulation codes focus on the modelling of plasma parameters like temperature and density for ions or neutrals. For example, NIMBUS [5] and EIRENE [6] are kinetic Monte-Carlo neutral transport codes, and B2 [7], EDGE-2D [8], UEDGE [9] and COREDIV [10] are fluid plasma codes for ions. Combinations of fluid and kinetic codes are for instance B2-EIRENE or SOLPS [11, 12]. Typically the plasma fluid codes are restricted to 2D, however, EMC3 [13] has 3D capability and is especially used for stellarators. The calculation of individual (plasma) particles is impossible due to the extremely large number of particles – in a fusion plasma the particle density is in the order of 10^{20} m^{-3} in the plasma centre and in the divertor – and thus other methods have to be applied. The fluid description of the plasma neglects the properties of individual particles and describes the whole system as fluid. This results in the fluid equations with the unknowns of density, pressure and flow (averaged) velocity of the electrons and ions. Also the electric and magnetic fields are included and the simultaneous solution of these equations leads to self-consistent results. The fluid theory is only valid for plasmas with high enough collisionality. A more general approach is done within the kinetic theory where the distribution function of electrons and ions is used. According to the statistical theory, the distribution function normally fulfils the Boltzmann equation. In sufficiently hot plasmas, collisions can be neglected and the Boltzmann relation becomes the so-called Vlasov equation. Consideration of the Coulomb collisions yields the Fokker-Planck equation. Within a strong magnetic field the gyro-kinetic description averages the motion over the gyration and the calculations become more efficient. A more detailed description of the different theories and simulation methods can be found for instance in [14] and references therein.
Modelling of the impurity transport and resulting erosion/deposition is treated by codes such as ERO [15], REDEP/WBC [16], EDDY [17], WallDYN [18], ASCOT [19] or DIVIMP [20]. These are 2D or 3D codes calculating the impurity transport based on the kinetic theory and/or following of guiding-centre orbits. Typically these code need the plasma background as input, which can come from measurements or from plasma simulations codes as mentioned above. DIVIMP can also be used to calculate plasma background parameters directly by means of an Onion Skin Model. Erosion processes and resulting deposition and material mixing are treated in different ways and levels of detail. The present contribution will focus on the ERO code – a brief description of ERO is presented in the following section 2.2.
The calculation of the electric field in front of plasma-exposed material surfaces is an important part of the impurity modelling: this field usually determines the main part of the incident ion energies, which then determine the amount of eroded material. It also strongly influences the near-surface transport of ions and the resulting deposition of eroded particles. The calculations of the electric field are done self-consistently with the Particle-In-Cell (PIC) method. Codes like BIT [21] and SPICE [22] are used for this purpose and also deliver ion fluxes and spatially resolved plasma parameters in the vicinity of surfaces.
The interaction of plasma particles and neutrals with the solid surface is treated by binary collision approximation codes like TRIM [23] (and its derivatives TriDyn and SDTrimSP [24]) and Molecular Dynamics based codes like PARCAS [25, 26]. Other models treat the impact of various types of power loads onto material surfaces and in particular consider extreme heat loads where for instance melting and melt layer motion, evaporation or brittle destruction appears. As examples the codes HEIGHTS [27], MEMOS [28] and PEGASUS [29] are mentioned here. The

problem of diffusion and its impact on the resulting fuel retention can be treated by some of these codes, however, also other specific codes are available like TMAP [30] or DIFFUSE [31].

2.2. Basics of the ERO code

ERO is a 3D Monte Carlo code modelling plasma-surface interaction processes and impurity transport within the edge plasma of fusion devices [32, 15]. Originally developed by Naujoks [33], it has been continuously further developed and applied to a large variety of fusion experiments, including predictive modelling of wall lifetime and tritium retention for ITER. Recently a major code revision to enhance code performance and to enable large scale simulations has been undertaken [34].

2.2.1. The simplified Scrape-Off Layer

The plasma in magnetically confined devices can be divided into a confined region within the last closed magnetic flux surface (LCMFS) and the scrape-off-layer (SOL) outside the LCFMS up to the wall elements. Typically the simulations cover the SOL and in some applications also part of the confined region. The plasma temperature, density and the parallel (to the magnetic field) background flow velocity are necessary parameters for the ERO simulations and can be delivered by measurements or plasma simulation codes. In many cases the variation of these parameters along the magnetic field lines is not provided. However, a simple SOL model [35] results in the following formulae for the parallel flow velocity and electron density:

$$v_{para}(s) = c_S \cdot \left(\frac{L_C}{2s} - \sqrt{\left(\frac{L_C}{2s}\right)^2 - 1} \right) \quad \text{with} \quad c_S = \sqrt{\frac{k(T¿¿e + T_i)}{m_D}}¿ \text{, } T_e \text{ and } T_i \text{ in K} \tag{1}$$

$$n_{e,\,para}(s) = \frac{s^2 / L_C}{L_C/2 - \sqrt{(L_C/2)^2 - s^2}} \tag{2}$$

Here s is the coordinate along the magnetic field with $s = 0$ at the stagnation point at which $v_{para} \rightarrow 0$, c_S is the acoustic sound speed (with T_e and T_i the electron and ion temperature, m_D the mass of plasma ions and k the Boltzmann constant) and L_C is the connection length. The parallel flow velocity reaches acoustic sound speed (Bohm criterion) when approaching the sheath entrance at $s = L_C/2$. The parallel density given in equation (2) is normalised to its value at the stagnation point $s = 0$, $n_{e,para}(s \rightarrow 0) \rightarrow 1$. It decreases by a factor of two at the sheath entrance compared to its value at the stagnation point. The parallel variation of the electron and ion temperature $T_{e,i}$ is usually neglected. The sheath entrance is assumed to be at the position of the surface if the details of the sheath are not resolved. This can be improved if PIC data are used as input to resolve the sheath structure (section 3.1.).

2.2.2. The electric field

First contribution is the electric field due to the sheath potential Φ_S. With some simplifications ($T_e = T_i$ and zero secondary electron emission coefficient), Φ_S can be approximated with $3kT_e/e$ (in V for T_e in K and e the elementary charge) for a deuterium plasma. In case of the magnetic field not perpendicular to the surface, the sheath potential Φ_S can be approximated as [36]:

$$\Phi_S(d) = \Phi_0 \cdot f_d(\alpha_B) \cdot e^{-d/2\lambda_D} + \Phi_0 \cdot \left(1 - f_d(\alpha_B)\right) \cdot e^{-d/r_L} \tag{3}$$

The total sheath is split into the electric sheath, which scales with the Debye length λ_D and the magnetic pre-sheath, which scales with the Larmor radius r_L of the plasma ions. In equation (3) d is the normal distance from the surface and the function $f_d(\alpha_B)$ determines the distribution of the sheath. For the magnetic field angle $\alpha_B = 0$ (i.e. B field perpendicular to the surface) f_d becomes one. With increasing α_B the function f_d approaches zero such that the magnetic part of the electric field becomes more and more dominant. More sophisticated approaches to calculate the sheath electric field based on PIC simulations will be shown in section 3.
A parallel electric pre-sheath field E_{para} arises inside the SOL from the parallel density gradient due to equation (2). This field is calculated from the force balance [37]:

$$E_{para}(s) = \frac{k \cdot T_e}{e} \cdot \left(\frac{L_C}{2s\sqrt{(L_C/2)^2 - s^2}} - \frac{1}{s} \right) \tag{4}$$

The parallel electric field drives positively charged ions to the direction of the surface. Thereby, ions with positive charge Q are accelerated to an energy ~ $0.5 \cdot Q \cdot kT_e/e$ when entering the electric sheath at $s \rightarrow L_C/2$, which coincides with the Bohm criterion.
Finally, a radial electric field $E_{rad}(r) = -d/dr\ \Phi_{para}(r)$ follows inside the SOL from the parallel electric field as the latter one causes an electric potential Φ_{para}, which depends on the radial co-ordinate r:

$$\Phi_{para}(r) = \frac{-k \cdot T_e(r)}{e} \cdot \left(\ln\left(L_C + \sqrt{L_C^2 - 4s^2} \right) - \ln\left(2L_C \right) \right) \tag{5}$$

Near to the surface the sheath electric field is the dominating contribution to the overall electric field. Away from the surface the sheath electric field strongly decreases as its potential scales with the small Debye length or the gyration radius of plasma ions and then the other contributions dominate. However, the potential drop of the sheath electric field is much larger than the ones from the pre-sheath and radial electric field. Therefore, in many cases the impact energy of ions hitting the surface is approximated to $E_{in} \sim 3 \cdot Q \cdot kT_e/e$. As mentioned before an energy of ~$0.5 \cdot Q \cdot kT_e/e$ adds up due to pre-sheath electric field and a typically smaller value due to the radial electric field. Also, for background ions the thermal energy due to the Maxwellian energy distribution has to be added. For eroded atoms returning to the surface, however, the impact energy depends on their ionisation length and thus can be smaller than $3 \cdot Q \cdot kT_e/e$ if ionisation takes place very near to the surface within the sheath. On the other hand, in the case of very high density plasmas, the friction between the impurity ions and the background plasma can become very effective leading to rather large impact energies. This has been discussed in more detail in [38].

2.2.3. Physical processes treated by ERO

According to the local plasma parameters a certain flux of background fuel and impurity particles hits the surface. The electron flux is given by:

$$\Gamma = n_e \cdot c_S \cdot \cos(\alpha_B) \tag{6}$$

Here n_e is the electron density at the sheath entrance. From this, the fluxes of fuel and impurities can be calculated. When the magnetic field is perpendicular to the surface normal, equation (6) delivers zero flux. In reality even at such conditions, which e.g. may occur at the tip of spherically shaped limiters, the flux hitting the surface can be non-zero e.g. due to cross-field diffusion and gyration effects – this can be considered in ERO by correction terms.

According to the impact energy and angle of the background particles, physical sputtering can be calculated according to [39]. However, normally the background plasma species are not followed in ERO, wherefore dedicated ERO runs can be performed to produce the impact angular distribution of background species. As the impact angular distribution depends on the magnetic field, plasma parameters and species, no general approach is possible. The physically sputtered particles are assumed to be neutrals and leave the surface with a Thompson energy distribution around the surface binding energy and a cut-off energy taking into account a maximum energy for sputtered particles given by the projectile´s impact energy. In most cases a cosine distribution relative to the surface normal and uniform distribution in the azimuthal plane are assumed for the angle of sputtered particles. However, other distributions can be considered. In the case of deuterium (or its isotopes) impact on carbon (C) or beryllium (Be) surfaces also chemical erosion or chemically assisted physical sputtering can be considered. Chemically eroded carbon particles leave the surface with Maxwellian energy distribution (around the surface temperature kT_{surf}). For beryllium, the energy comes from Molecular Dynamics calculations. In both cases (C and Be) an angular distribution similar to physically sputtered particles is assumed.
The transport of impurity particles is done in the test particle approximation – the properties of the given background plasma are thus not affected by the impurities. The test particles leave the surface as neutrals and move along straight lines unless neutral collisions are considered.
Ionisation, dissociation and recombination are considered with rate coefficients for the different processes, mainly based on ADAS [40]. After ionisation, the friction with the background ion flow along the magnetic field lines due to Coulomb collisions is calculated by means of the relaxation times. As the background flow near to the surface is directed towards the surface, the friction drives the impurity ions towards the surface. In fusion experiments strong temperature gradients can develop along the magnetic field lines leading to a thermal force, which acts in the direction of the temperature gradient along the B field and therefore opposite to the friction force. Near to surfaces it thus typically drives positively charged ions away from the surface. The thermal force can be written as [41]:

$$F_{thermal} = \alpha \cdot \frac{dT_e}{dl} + \beta \cdot \frac{dT_i}{dl} \quad \text{with } l \text{ the distance from the surface along the magnetic field} \qquad (7)$$

The coefficients α and β can be calculated according to formulae provided in [41] and references therein. Usually in ERO the temperatures are assumed to be constant along the magnetic field, however, to account for thermal force effects the gradients in (7) are calculated along the B field according to formulae from literature, see e.g. [42]. As the conductivity of electrons is typically much greater than the one of ions, the electron temperature gradient is normally neglected. The movement due to the Lorentz force in the electric and magnetic field E, B is calculated according to the Boris method [43] wherefore drifts due to E and B are automatically included. Finally, cross field diffusion is considered by changing the position of the test particle in dependence on an input cross-field diffusion coefficient.
The impact energy and angle of traced test particles hitting the surface is calculated by ERO and thus can be used to evaluate the physical sputtering according to [39]. The assumptions of energy and angular distribution of the newly sputtered particles are the same as for sputtering by background particles. When a traced test particle hits the surface the probability of deposition is calculated according to the reflection coefficient R. The reflection coefficient R for atomic species depends on impact angle and energy and is determined by means of a pre-calculated data base from TRIM or MD simulations. Reflection of molecular species is defined by input

parameters for the reflection coefficient, the energy distribution of reflected species and the type of reflected species. Alternatively, if available, calculated data can be used (e.g. based on MD simulations). The energy and angle of the reflected atomic species are determined again with TRIM-based data. Impurities in the background plasma (e.g. beryllium or carbon) can be deposited on the surface with a probability of deposition determined in the same way as for traced test particles. However, as background species normally are not followed by ERO simplified assumptions in form of mean values for impact angle and energy can be made. Optionally, this can be improved by dedicated ERO runs where background impurities are followed to calculate their distribution of impact angle and energy.
A simple homogenous mixing model (HMM) is implemented in ERO to address the mixing of different species at the surface. The surface is divided into an interaction layer and a bulk volume, which serves as a particle reservoir. Erosion and deposition only takes place within the interaction layer. It is assumed that the number of particles is constant within the interaction layer. The ERO code can be coupled with the SDTrimSP code [44]. Using this option material mixing is addressed automatically with SDTrimSP instead of the above-described simple mixing model. Also, the amount of physical sputtering and reflection is calculated by SDTrimSP instead of using yields from pre-calculated data bases. It has been seen that the coupled ERO-SDTrimSP version produces similar results as the ERO-HMM version if the mixed species have similar atomic numbers [44]. However, mixing of particles with very different masses involves additional effects, which can only be treated by SDTrimSP.

3. Prompt deposition modelling with the ERO code

Tungsten is used for the divertor of ITER and is also under discussion as plasma-facing material for DEMO. In addition to its low physical sputtering, tungsten also has a high melting point. However, the amount of tungsten in the core plasma has to be minimised due to its strong ability for plasma dilution and cooling. The property of so-called prompt deposition of high-Z materials like tungsten could help to reduce the net erosion. Prompt deposition originally means the deposition of eroded atoms during their first gyration after erosion [45]. The high ionisation rate coefficient and therefore small penetration into the plasma in combination with the large gyration radius of tungsten suggests a large fraction of prompt deposition. Within the present contribution the term “prompt deposition” is used in a slightly different way as ions near to the surface within the strong electric field of the sheath normally do not follow a clear gyration motion anymore. Here, eroded particles are defined as promptly deposited if the time needed to return to the surface is smaller than the gyration time. In the following various parameter studies are presented to investigate the processes governing the amount of prompt deposition. In particular, the influence of the sheath properties will be analysed. First results have been published in [38, 46] and the present work is an extension of the simulations shown therein. Erosion and prompt deposition of tungsten has been investigated in various devices, e.g. in ASDEX-Upgrade [47] and JET-ILW [48]. The influence of the electric field and the density drop within the sheath also have been studied in [49] on the example of tungsten and molybdenum deposition in dedicated DIII-D experiments.

3.1. Parameter studies

The geometry used for the following simulations is shown in figure 1 together with exemplary simulation results of tungsten neutral and ion density above the surface. The surface has an inclination angle of 2° relative to the magnetic field (3 T, parallel to the x-direction). To simulate tungsten (W) sputtering, W particles are injected at the centre of the surface with a Thompson energy distribution around the W binding energy (8.8 eV) and a cosine angular distribution. The

injected particles are followed within the simulation box with extensions of 1000 mm in x-direction, 100 mm in y-direction and 100 mm in z-direction. Particles leaving this box are lost and not further followed. The dotted line in figure 1 indicates the separation between the SOL and the confined plasma. If no PIC data are used for the sheath description, the electron and ion temperature is assumed to be constant inside the simulation volume. Also the electron density is constant except of a variation inside the SOL along the B field according to equation (2). For non-PIC cases, the flow velocity inside the SOL is described with equation (1) and set to zero inside the confined plasma. For the connection length L_C a value of 20 m has been assumed. The thermal force and the electric fields are calculated according to equations described in section 2.

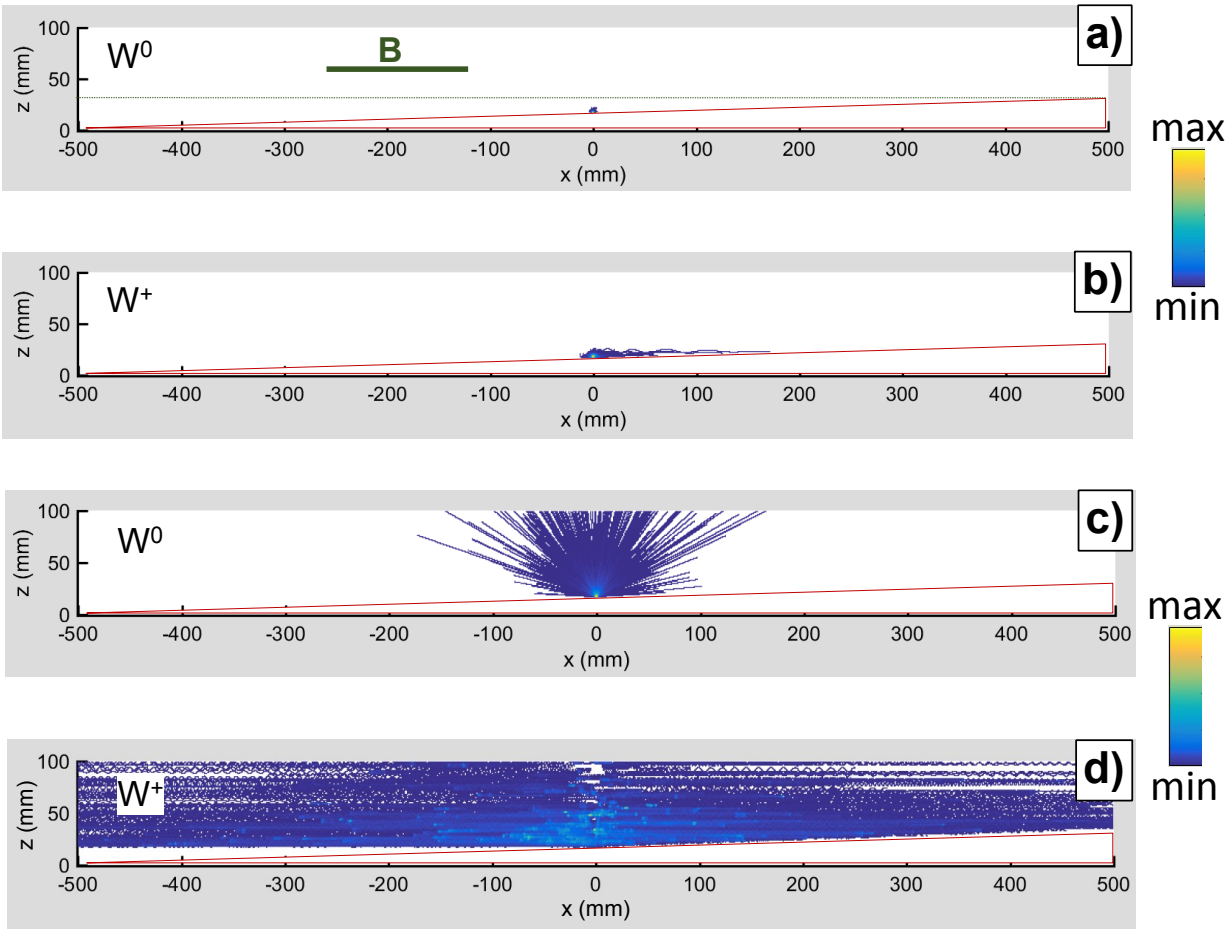

Figure 1 *Simulation geometry and examples of neutral and singly ionised tungsten distribution above the surface. a), b) correspond to case 2 (see table 1) with high electron density and c), d) to case 4 with low electron density. The electron temperature of 5 eV is the same for both cases.*

For the simulations applying PIC data for the sheath description, the plasma parameters, sheath electric field, flow velocity and thermal forces are taken from the PIC calculations carried out with the BIT1 code and used as input into ERO. Outside the sheath the same assumptions have been made as for the ERO cases without using PIC data as input. W particles returning to the

surface are assumed to be deposited (reflection is neglected) to study the amount of returning particles. Also, self-sputtering due to returning ions is not considered here but has been studied in [46] showing that runaway sputtering typically does not occur. Ionisation data for neutral W are taken from [50] and for higher ionisation states from [51].

case #	T_e(eV) at sheath entrance	n_e (cm^{-3}) at sheath entrance
1	20	6E13
2	5	6E13
3	20	5E11
4	5	5E11

Table 1 *Plasma parameters used for the prompt deposition studies.*

Simulations are carried out for 4 different plasma conditions summarised in table 1. As an example figure 2 shows the electron temperature and density variation within the sheath for case 2 resulting from BIT1 PIC simulations (denoted with "PIC") in comparison to the simple assumptions in ERO (denoted with "SIMPLE") when no PIC data are used. The distance d is perpendicular to the surface. It is seen that temperature and density decrease within the sheath when approaching the surface, the sheath entrance is located at d ~ 8 mm for case 2. In contrast, the temperature with the simple assumption is constant and the density only shows a slight decrease according to formula (2). It has to be stressed again that the location of the surface at d = 0 equals the position of the sheath entrance for the simple assumptions as the plasma variation inside the sheath is not resolved. For all 4 cases the overall sheath potential drop from the PIC simulations corresponds rather well to the simplified assumption of $3kT_e/e$ (= 15 V for T_e = 5 eV) whereas the detailed spatial variation can differ from the one given in equation (3), see figure 3 as an example again for the plasma conditions of case 2.

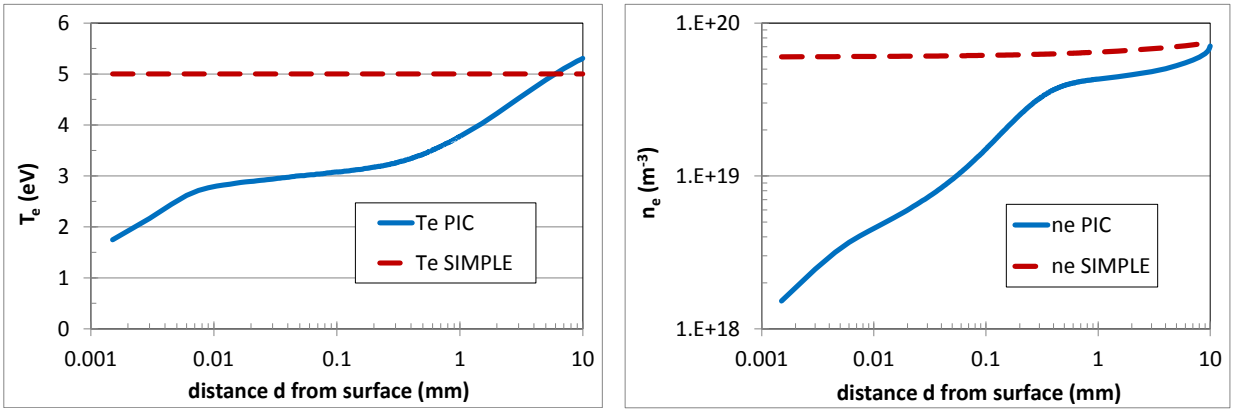

Figure 2 *Electron temperature (left) and density (right) inside the sheath from PIC (BIT1 code) in comparison to simple assumptions. The parameters correspond to plasma conditions of case 2 from table 1.*

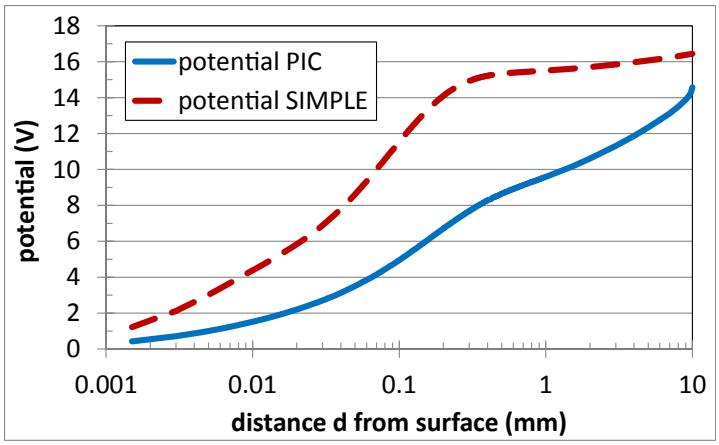

Figure 3 *Sheath potential from PIC (BIT1 code) in comparison to simple assumptions according equation (3) for the plasma conditions of case 2 from table 1.*

Impact of the cut-off energy

To study the influence of the cut-off energy for the Thompson distributed W particles various cut-off energies have been studied for the energy distribution of injected W atoms. For cases 1 and 3 cut-offs of 50, 100, 200 and 300 eV and for cases 2 and 4 cut-offs of 10, 20, 40 and 80 eV have been used. These energies cover the deuterium ion impact energy distribution computed by the corresponding PIC simulations. Figure 4 summarises the prompt W deposition fractions from the ERO simulations with input of PIC data for the sheath properties. First of all the general trend of increasing prompt deposition with increasing electron temperature and density is obvious, which results from decreasing penetration of W atoms into the plasma. Furthermore it is seen that for the plasma conditions of case 1 and 2 (high density) the amount of prompt deposition decreases with increasing cut-off energy: for case 1 from ~94% to ~88% and for case 2 from ~63% to 56%. In contrast, the cut-off energy does not have any significant effect in the low density cases 3 and 4 indicating that under these conditions only particles with very small starting energy can be promptly deposited. The same study of cut-off energy has been performed with ERO simulations without using PIC sheath and reveals similar trends.

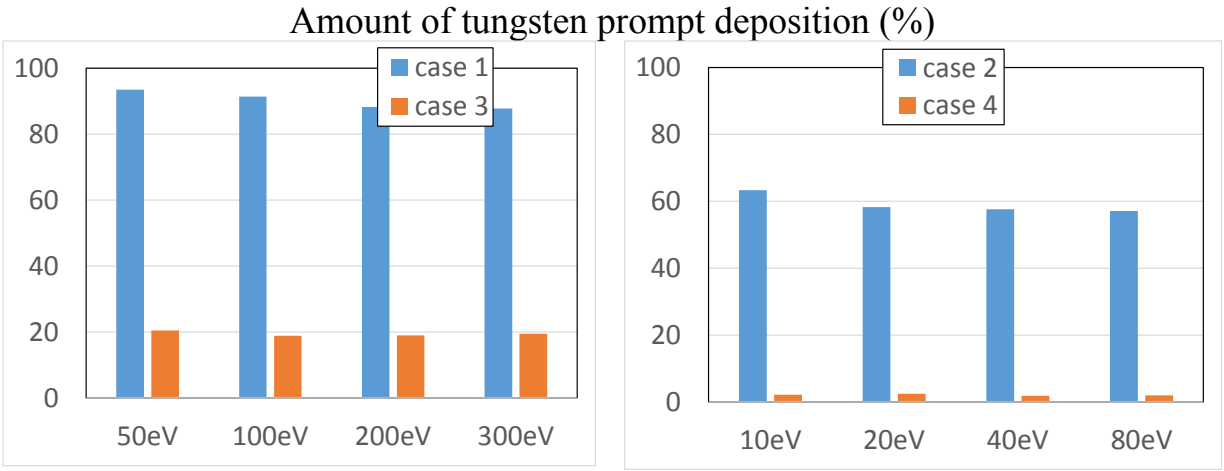

Figure 4 *Simulated amount of prompt deposition for the different plasma conditions from*

table 1 in dependence on the cut-off energy. PIC data have been used for the description of the sheath.

Impact of spatially resolved sheath

The simulated results of the amount of prompt tungsten deposition from ERO using PIC data for the sheath (ERO-PIC) are compared with ERO results applying the simple assumptions for the sheath (ERO-SIMPLE). The simulations have been done for the plasma conditions case 1–4, each for the cut-off energies discussed in the previous paragraph. With these, the overall resulting prompt deposition has been calculated as the average of the individual results weighted with a factor according to the impact deuterium ion energy distribution calculated with PIC. Figure 5 shows that in all cases ERO-PIC leads to smaller amount of tungsten prompt deposition. This can be explained by the decay of electron density and temperature within the sheath calculated by PIC leading to larger ionisation length of the tungsten atoms. The relative difference in the simulated values is about 5% for the high temperature cases 1 and 3 and about 30% for the low temperature cases 2 and 4. Also, as seen before, both ERO-PIC and ERO-SIMPLE simulations lead to an increase of prompt deposition with increasing electron temperature and density.

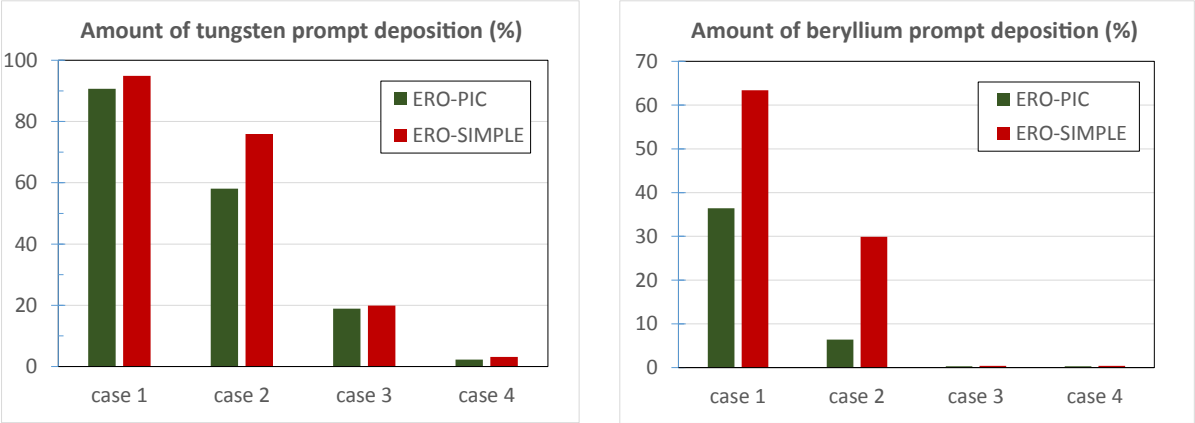

Figure 5 *Simulated amount of prompt deposition for the different plasma conditions from table 1: comparison of ERO-PIC with ERO-SIMPLE. Left: tungsten and right: beryllium.*

The overall deposition of tungsten, i.e. including also non-prompt deposition, calculated from ERO-PIC and ERO-SIMPLE is 100% for the high density cases 1 and 2. For the low density cases 3 and 4 ERO-PIC results in larger overall tungsten deposition compared to ERO-SIMPLE (65% vs. 34% for case 3 and 24% vs. 18% for case 4). The main reason here is a larger thermal force in ERO-SIMPLE compared to ERO-PIC leading to a larger fraction of W particles leaving the simulation box.

Comparison of tungsten with beryllium deposition

Simulations have been also performed with beryllium for comparison. Ionisation data are taken from ADAS [40]. For the Thompson distribution the beryllium binding energy of 4.4 eV is used. The simulations results are presented in figure 5 and show significantly smaller prompt deposition compared to tungsten as the low-Z material beryllium has smaller ionisation probability and also the gyration radius is smaller. However, the general trends are similar as for tungsten, although the differences in the prompt deposition between ERO-PIC and ERO-

SIMPLE for the plasma conditions of cases 1 and 2 are larger whereas both, ERO-PIC and ERO-SIMPLE, lead to negligible prompt deposition for the cases 3 and 4. As for tungsten, also for beryllium the overall deposition in the high density cases 1 and 2 is 100%. For the cases 3 and 4 the overall beryllium deposition is lower and lying between 1% and 10%.

3.2. Prompt tungsten deposition under JET divertor conditions

The erosion and deposition of tungsten along a divertor tile is modelled for typical JET intra-ELM conditions and for L-mode (or equivalent inter-ELM) conditions where the erosion is determined by impurity ions. A qualitative comparison of simulated prompt tungsten deposition will be done with the data from [48]. The simplified simulation geometry is shown in figure 6. The simulation box has lengths of 150 mm along and vertical to the tile. The vertical direction corresponds to the radial direction of the tokamak. Perpendicular to the plane shown in figure 6 the volume has an extension of 16 m in toroidal direction neglecting the toroidal curvature. The magnetic field of 2.5 T lies within the separatrix almost in toroidal direction with a magnetic field angle of $\alpha_B \sim 85°$ relative to the surface normal.

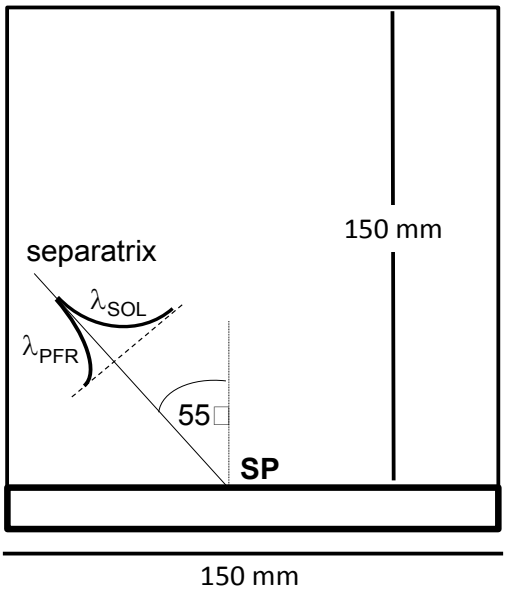

Figure 6 *Geometry used for the W erosion/deposition modelling along a divertor tile.*

The plasma parameters ($T_e = T_i = T$ and $n_e = n_i = n$) are assumed to be constant within the separatrix and decay exponentially with different decay lengths $\lambda_{SOL}(T) = 110$ mm, $\lambda_{PFR}(T) = 25$ mm and $\lambda_{SOL}(n) = 27$ mm, $\lambda_{PFR}(n) = 16$ mm towards the SOL and the private-flux region (PFR). The decay lengths λ are based on Langmuir probe measurements of typical L-Mode discharges [52]. Along the toroidal direction the plasma parameters are kept constant. According to [48] the strike point temperatures and densities range within 20 to 50 eV and 5E12 to 1E13 cm^{-3} for the prompt deposition study. The flow velocity variation along the magnetic field (assuming connection length L_c of 30 m), the electric fields and the thermal force are described as presented

in section 2. To calculate the radial electric field from equation (5) an exponential radial decay length of 20 mm for T_e is assumed. No PIC data will be used for the sheath description as the plasma parameters spatially vary along the divertor tile and PIC data are not available for all these different conditions – in the future 2D PIC simulations would be desirable. Besides these L-Mode like conditions also H-mode like parameters are studied. For this purpose, at the strike point T_e = 50 eV, T_i = 1000 eV and $n_e = n_i$ = 5E13 cm^{-3} are assumed during the ELM together with the same decay lengths as for the L-Mode condition, i.e. experimentally observed profile broadening during ELMs is not considered here. Instead of Maxwellian distributed ions the deuterium ion energy is set to T_i. The such-defined ELM parameters are similar to those in [53] and correspond to the so-called streaming model [54]. For the inter-ELM conditions the parameters from the L-Mode are applied. The duration of the ELM phase determined by MHD crash is assumed to be 500 µs and the ELM frequency is set to 10 Hz [48]. A constant concentration of 0.5% [48] Be^{2+} relative to the deuterium D^+ flux is assumed to hit the surface. Reflection of returning W particles and W self-sputtering is not considered. Also, Be deposition from the background and resulting material mixing at the surface is neglected as the present study focus on the (prompt) deposition modelling of tungsten. The later was confirmed after extraction of the tile as no significant net Be deposition was found on the JET target after hours of plasma operation.

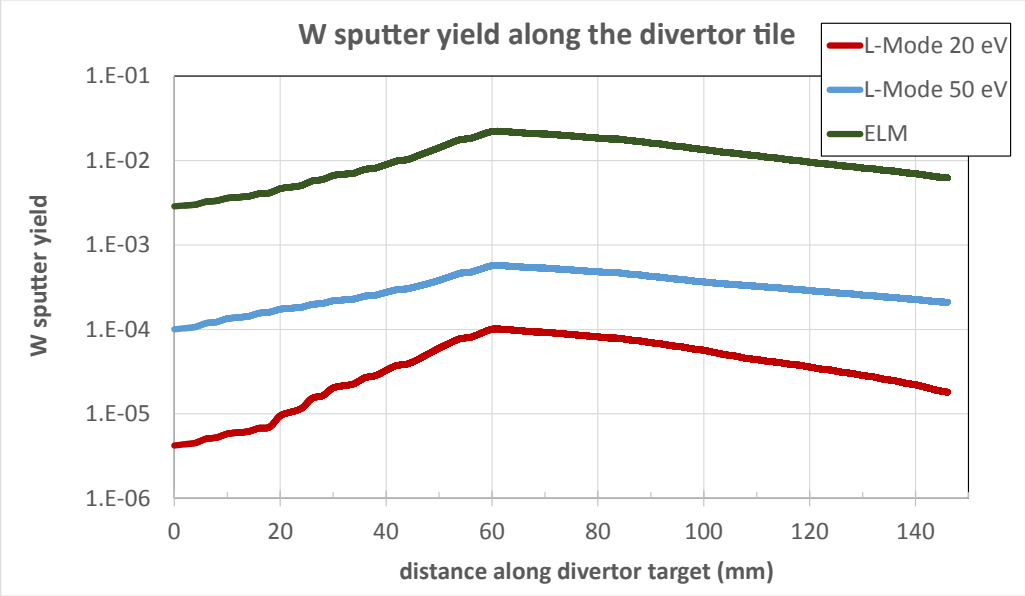

Figure 7 *Effective tungsten sputter yields for L-Mode (strike point temperature of 20 eV and 50 eV) and ELM conditions along the divertor tile.*

Figure 7 shows the effective sputtering yields Y_{eff} along the divertor tile for L-Mode conditions with strike-point temperatures of 20 and 50 eV and for ELM conditions. Effective yield here means the ratio of sputtered W atoms and total impinging flux of D and Be ions. The sputter yields for D^+ on W and Be^{2+} on W for the L-Mode conditions are based on SDTrimSP calculations assuming 60° impact angle and considering Maxwell distributed impact energy and acceleration in the sheath potential. For the ELM conditions a mono-energetic impact is assumed with $E_{in} = m_{proj}/m_D \times T_i$ where m_{proj} is the mass of deuterium or beryllium. To estimate the impact angle of ions hitting the target during ELM conditions, dedicated ERO runs have been performed following background D^+ and Be^{2+} ions until reaching the surface. These simulations show that

the mean impact angle is between 60° and 85° with larger angle for higher impact energies. SDTrimSP simulations with these energy and angular information have been done to obtain the sputter yields during ELM conditions. Sputtering during L-Mode is dominated by Be ions as the deuterium ion impact energies are below or near to the threshold for W sputtering. The Y_{eff} during ELM are much greater than the ones for the L-Mode conditions. Due to the large impact energy during ELM, D ions now dominate the overall W sputtering (only about 20% of the sputtering is due to Be ions). At the strike point, Y_{eff} for ELM is about a factor of 40 larger than the one for the L-Mode condition with 50 eV and a factor of about 220 for the L-Mode with 20 eV.

The resulting W gross erosion rates for inter-ELM (i.e. L-Mode) conditions with two strike point temperatures (20 and 50 eV) and densities (5E12 and 1E13 cm^{-3}) are compared with the rates from the ELM condition and shown in figure 8. For this evaluation the ELM frequency and duration have been considered to get the erosion per second. The ELM erosion dominates all four intra-ELM erosion rates with factors between 3 and 60. For a specific H-mode example at JET [48], this ratio has been determined to 9 and thus agrees rather well with the range resulting from the simulations presented here. Finally the modelled net erosion profiles of tungsten are displayed in figure 9 for one example of inter-ELM conditions (50 eV, 5E12 cm^{-3}) and the intra-ELM phase.

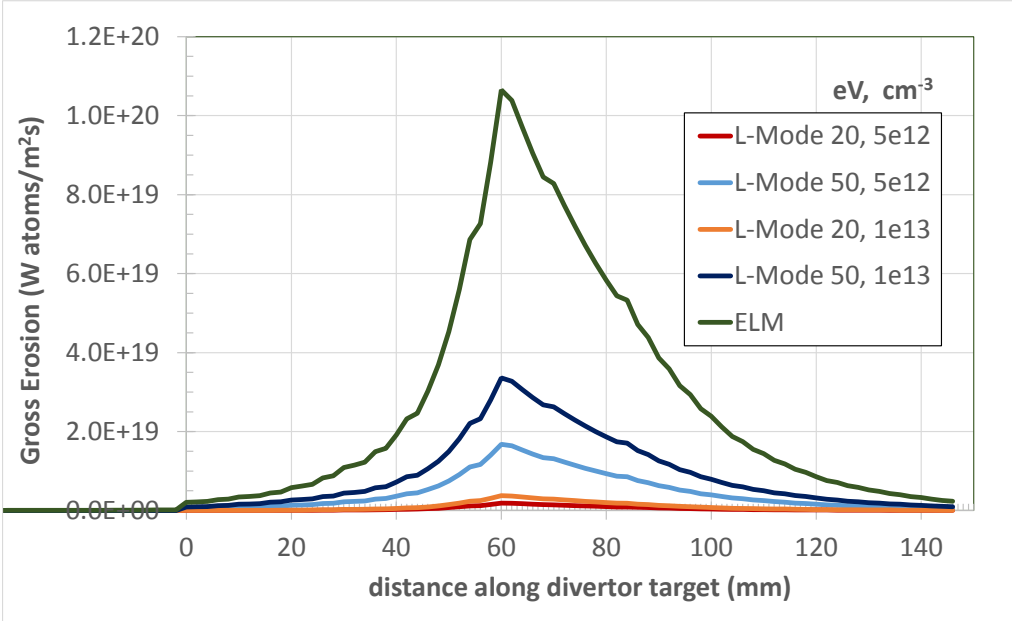

Figure 8 *Tungsten gross erosion rate along the divertor tile: four L-Mode in comparison to ELM conditions.*

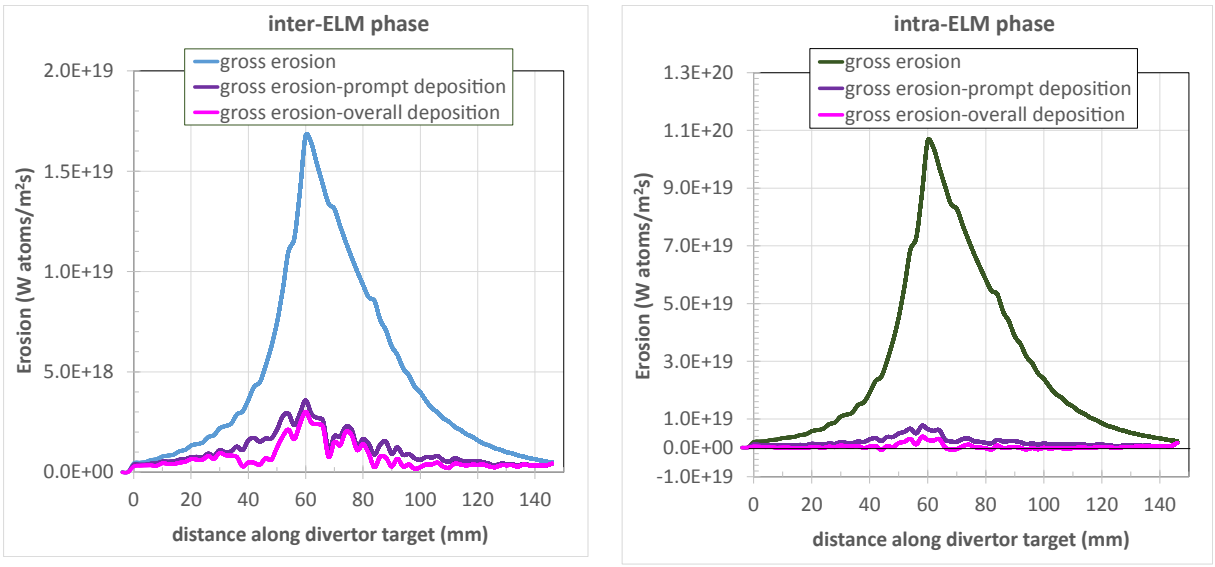

Figure 9 *Gross and net erosion profiles along the divertor tile: inter-ELM (left) with 50 eV and 5E12 cm^{-3} at the strike point vs. intra-ELM (right) phase.*

The W erosion is strongly reduced by deposited tungsten particles. For instance, the W erosion rate at the strike point due to the ELM is lowered from about 1E20 W atoms/m^{2}s gross erosion to about 3E18 W atoms/m^{2}s net erosion. The averaged (over the tile) fraction of prompt deposition is about 77% for the inter- and 93% for the intra-ELM phase. In addition to prompt deposition, further eroded particles are non-promptly deposited on the tile resulting in an overall amount of W deposition of 84% for inter- and 98% for intra-ELM condition. The lower limit of the (prompt) deposition of tungsten has been estimated in [48] by spectroscopy for L-Mode conditions similar to the plasma assumptions made here. The resulting value of 50% is well in line with the simulations presented here. The large deposition during ELM conditions is a result of the high density.

First ERO simulations of W erosion and deposition within the divertor of JET have been already presented in [55]. Therein the thermal force as well as the radial and parallel electric fields have been neglected. To study their influence in the present work they have been switched off for one example of plasma parameters (50 eV, 5E12 cm^{-3}). It is seen that the overall tungsten deposition increases from 84% to 95% when the thermal force is switched off whereas the amount of prompt deposition is almost unaffected. Neglecting in addition the radial and parallel electric fields does not significantly change the amounts of overall and prompt W deposition.

4. Conclusions and Outlook

The basics of the plasma-wall interaction and impurity transport code ERO have been described. The application of the code has been demonstrated on the example of tungsten prompt deposition. Parameter studies revealed the influence of the plasma parameters on the deposition. The spatially resolved properties of the sheath in front of surfaces have been calculated with PIC simulations and used as input for ERO. The PIC simulations calculate a decrease of the electron temperature and density when approaching the surface, which is not included in the ERO simulations without resolved sheath properties (ERO-SIMPLE), which reduces the prompt tungsten deposition up to 30%. The overall deposition including non-promptly deposited tungsten reaches 100% at the high electron density studied both for ERO-PIC and ERO-

SIMPLE. For the low density ERO-PIC leads to lower overall deposition with a reduction of up to 50% - this is mainly due to larger thermal force assumed in ERO-SIMPLE.
Simulations of tungsten erosion and deposition have been presented for inter- and intra-ELM conditions in the divertor. A comparison with JET data has shown that the gross erosion of tungsten can be reproduced. As in the experiment the gross W erosion is dominated by the intra-ELM phase. Moreover, the simulated amount of (prompt) deposition is in agreement with experimental estimations of the lower limit. The deposition leads to a strong reduction of the gross erosion, e.g. a factor of about 30 at the strike point under intra-ELM and about 5 under inter-ELM conditions is obtained from the simulations. In the future further simulations are planned for selected JET discharges including the benchmark of modelled W light emission with spectroscopic observations. Also so far neglected reflection of W particles, self-sputtering and material mixing will be included. The influence of PIC sheath data under divertor conditions will also be studied.

Acknowledgements
This work has been carried out within the framework of the EUROfusion Consortium and has received funding from the Euratom research and training programme 2014–2018 under grant agreement No 633053. The views and opinions expressed herein do not necessarily reflect those of the European Commission. This work has been done under WP PFC.

References
[1] A. Kirschner, Transactions of Fusion Science and Technology 57 (2010) 277
[2] J. Roth et al., J. Nucl. Mat. 390–391 (2009) 1
[3] S. Brezinsek, JET-EFDA contributors, J. Nucl. Mat. 463 (2015) 11
[4] M. Shimada et al., J. Nucl. Mat. 438 (2013) S996
[5] E. Cupini, *Nimbus: Monte Carlo Simulation of Neutral Particle Transport in Fusion Devices – Part One, Physical Model and Numerical Method*, Commission of the European Communities, 1983
[6] D. Reiter, M. Baelmans and P. Börner, Fusion Science and Technology 47 (2005) 172
[7] B.J. Braams*, A multifluid code for simulation of the edge plasma in tokamaks*, Report under NET Contract No. 142/83-11/FU-NL/NET (1987)
[8] R. Simonini, A. Taroni, M. Keilhacker, G. Radford, J. Spence, G. Vlases, M.L. Watkins, S. Weber, J. Nucl. Mat. 196–198 (1992) 369
[9] T.D. Rognlien, J.L. Milovich, M.E. Rensink, G.D. Porter, J. Nucl. Mat. 196–198 (1992) 347
[10] R. Stankiewicz, R. Zagórski, J. Nucl. Mat. 313–316 (2003) 899
[11] S. Wiesen et al., J. Nucl. Mat. 463 (2015) 480
[12] A.V. Chankin et al., Plasma Phys. Control. Fus. 48 (2006) 839
[13] Y. Feng, F. Sardei, J. Kisslinger, P. Grigull, K. McCormick, and D. Reiter, Contrib. Plasma. Phys. 44 (2004) 57
[14] F.F. Chen*, Introduction to plasma physics and controlled fusion. Volume 1: Plasma physics*, Springer, 1984
[15] A. Kirschner, V. Philipps, J. Winter, U. Kögler, Nucl. Fusion 40 (2000) 989
[16] Jeffrey N. Brooks, Fusion Eng. Des. 60 (2002) 515
[17] K. Ohya, Phys. Scripta T124 (2006) 70
[18] K. Schmid, M. Reinelt, K. Krieger, J. Nucl. Mat. 415 (2011) S 284
[19] J. A. Heikkinen and S. K. Sipilä, Physics of Plasmas 2 (1995) 3724

[20] P.C. Stangeby, J.D. Elder, J. Nucl. Mat. 196–198 (1992) 258
[21] D. Tskhakaya, M. Groth, JET EFDA contributors, J. Nucl. Mat., 463 (2015) 624
[22] R. Dejarnac, J.P. Gunn, J. Nucl. Mat. 363–365 (2007) 560
[23] W. Eckstein, *Computer simulation of ion-solid interaction, Springer*, Berlin (1991)
[24] W. Eckstein, R. Dohmen, A. Mutzke, R. Schneider, *SDTrimSP: A Monte-Carlo code for calculating collision phenomena in randomized targets,* Report IPP, 12/3 (2007)
[25] K. Nordlund**,** M. Ghaly, R.S. Averback, M. Caturla, T. Diaz de la Rubia, J. Tarus, Phys. Rev. B 57 (1998) 7556

[26] K. Nordlund, M. Ghaly, R.S. Averback, J. Appl. Phys. 83 (1998) 1238
[27] A. Hassanein, I. Konkashbaev, J. Nucl. Mat. 273 (1999) 326
[28] B. Bazylev et al., Phys. Scripta, T128 (2007) 229
[29] S. Pestchanyi and H. Würz, Phys. Scripta T 91 (2001) 84
[30] G.R. Longhurst, *TMAP7 User Manual*, INEEL/EXT-04-02352, Dec. 2008
[31] K.L. Wilson, M.I. Baskes, J. Nucl. Mat. 76–77 (1978) 291
[32] U. Kögler, J. Winter*, ERO-TEXTOR: 3D Monte Carlo code for local impurity modeling in the scrape-off layer of TEXTOR*, Jülich Report Jül-3361, 1997, ISSN 0944-2952
[33] D. Naujoks, R. Behrisch, J.P. Coad, L.C.J.M. De Kock, Nucl. Fusion 33 (1993) 581
[34] J. Romazanov et al., *First ERO2.0 modelling of Be erosion and non-local transport in JET ITER-like Wall*, submitted to Phys. Scripta
[35] P.C. Stangeby, G.M. McCracken, Nucl. Fusion 30 (1990) 1225
[36] J.N. Brooks, Phys. Fluids B2 8 (1990) 1858
[37] M.Z. Tokar, Contrib. Plasma Phys. 36 (1996) 250
[38] A. Kirschner, D. Tskhakaya, G. Kawamura, D. Borodin, S. Brezinsek, R. Ding, Ch. Linsmeier and J. Romazanov, Contrib. Plasma Phys. 56, No. 6-8 (2016) 622
[39] W. Eckstein, Vacuum 82 (2008) 930
[40] H.P. Summers, *The ADAS User Manual, version 2.6* (2004), http://www.adas.ac.uk
[41] J. Neuhauser, W. Schneider, R. Wunderlich, K. Lackner, Nucl. Fusion 24 (1984) 39
[42] P.C. Stangeby, J.D. Elder*,* Nucl. Fusion 35 (1995) 1391
[43] C.K. Birdsall & A.B. Langdon, *Plasma physics via computer simulation*, The Adam Hilger series of plasma physics, IOP Publishing Ltd, 1991
[44] S. Droste, A. Kirschner, D Borodin, A Kreter, S Brezinsek, V Philipps, U Samm, O Schmitz and the TEXTOR team, Plasma Phys. Control. Fus. 50 (2008) 015006
[45] D. Naujoks, J. Roth, K. Krieger, G. Lieder, M. Laux, J. Nucl. Mat. 210 (1994) 43
[46] A. Kirschner, D. Tskhakaya, D. Borodin, S. Brezinsek, J. Romazanov, R. Ding, Ch. Linsmeier, *Modelling of Prompt Deposition of Tungsten under Fusion Relevant Conditions*, contribution to 26th IAEA Fusion Energy Conference, THP/6-22 (2016)
[47] R. Dux et al., J. Nucl. Mat. 390-391 (2009) 858
[48] G.J van Rooij et al., J. Nucl. Mat. 438 (2013) S42
[49] R. Ding et al., Nucl. Fusion 56 (2016) 016021
[50] L.A. Vainshtein, I. Beigman, Ph. Mertens, S. Brezinsek, A. Pospieszczyk and D. Borodin, J. Phys. B: At. Mol. Opt. Phys. 44 (2011) 125201
[51] M. Higgins, J.G. Hughes, H.B. Gilbody, F.J. Smith, M.A. Lennon, K.L. Bell, A.E. Kingston, *Atomic and molecular data for fusion, Part III: recommended cross sections and rates for electron ionisation of light atoms and ions: copper to uranium*, Tech. Rep. CLM–R294, Culham Laboratory, Abingdon, Oxfordshire, UK (1989)
[52] K. Krieger et al., J. Nucl. Mat. 390–391 (2009) 110

[53] C. Guillemaut et al., Phys. Scripta T167 (2016) 014005
[54] W. Fundamenski, R.A. Pitts and JET EFDA contributors, Plasma Phys. Control. Fus. 48 (2006) 109
[55] A. Kirschner et al., J. Nucl. Mat. 463 (2015) 116